communications earth & environment

ARTICLE

https://doi.org/10.1038/s43247-021-00143-5 OPEN

Changes in the Gulf Stream preceded rapid warming of the Northwest Atlantic Shelf

Afonso Gonçalves Neto [1✉], Joseph A. Langan [1] & Jaime B. Palter [1]

The Northwest Atlantic Shelf provides ecological and economic benefits along the heavily populated North American coastline and beyond. In 2009-2010, abrupt warming prompted an ecosystem shift with consequences for fisheries, yet the cause of this event is unclear. Here we use satellite altimetry and in situ measurements to show that, in 2008, the Gulf Stream migrated closer to the Tail of the Grand Banks, a shift that has persisted ever since. This change reduced the westward connectivity of the Labrador Current that otherwise supplies cold, fresh, oxygen-rich waters to the shelf. Within one year after the appearance of anomalously warm and saline water at the Tail of Grand Banks, subsurface warming progressed south-westwards. Historical observations suggest a similar sequence of events may have occurred in the 1970s. Therefore, monitoring water properties at the Tail of Grand Banks may offer predictability for shelf properties and ecosystem perturbations with substantial lead time.

[1] Graduate School of Oceanography, University of Rhode Island, Narragansett, RI 02882, USA. ✉email: afonso@uri.edu

The Northwest Atlantic Shelf is among the fastest warming regions in the global ocean[1] (Fig. 1). This region is home to ecologically and economically valuable marine species, including the American lobster and the Atlantic sea scallop—two of the most valuable single-species fisheries in the United States[2]. The Northwest Atlantic surface warming during at least the past 4 decades has been attributed to both natural and anthropogenic forcing[3], and has been enhanced in recent years by atmospherically driven extreme events[4,5]. Shelf bottom waters have also warmed in recent decades, but with distinct temporal and spatial patterns when compared to the surface warming, suggesting that different forcing factors are likely at play here[6]. In one high-resolution model, simulated warming events in the Northwest Atlantic are strongly correlated with negative anomalies in the strength of the Atlantic Meridional Overturning Circulation (AMOC), leading to the interpretation that recent and historic warming in this region is an indicator of AMOC slowing in the 20th century[7]. Under continuous greenhouse gas emissions, the AMOC slowdown and the associated warming of the Northwest Atlantic[8] are expected to increasingly alter historically exploited stocks in this region, demanding adaptation of fisheries risk assessments to maintain resilience in a changing climate[9,10].

The Northwest Atlantic is also the locale where the swift, deep-reaching Gulf Stream and Labrador Current are in close proximity, as they transport warm, salty subtropical water poleward and cold, fresh Labrador Sea Water equatorward, respectively (see schematized currents in Fig. 1). In this region, some of the longest continuous records of ocean temperature and salinity have been collected, several dating to before the turn of the 20th century. More than 50 years ago, these records had already revealed that the sea surface temperature could fluctuate by up to 2 °C on a decadal timescale over a region extending at least from the coast of New Jersey, US to Halifax, Canada[11]. Subsequent research linked these temperature fluctuations to ripples through the food web and fisheries[1,12–16], and showed that one of their drivers may be a modulation in the westward transport of the Labrador Current south of the shallow underwater plateau known as the Grand Banks of Newfoundland[17–19] (see Fig. 1 for currents and landmarks).

More recently, a high-resolution model simulation suggested that the decreasing proportion of Labrador Current water on the Northwest Atlantic Shelf coincides with a deepening thermocline at the crossroads of the subtropical and subpolar circulation at the Tail of the Grand Banks (TGB)[20]. Despite the long history of observations and these more recent model results, a description of the mechanisms involved in the rapid warming of the Northwest Atlantic Continental Shelf has been lacking, hindering our ability to predict these changes in advance. Here we connect abrupt migrations in the Gulf Stream position to the warming of the Northwest Atlantic Shelf and provide an observation-based assessment of the predictability of shelf property changes. Such predictability may ultimately improve forecasts of ecosystem changes in this region.

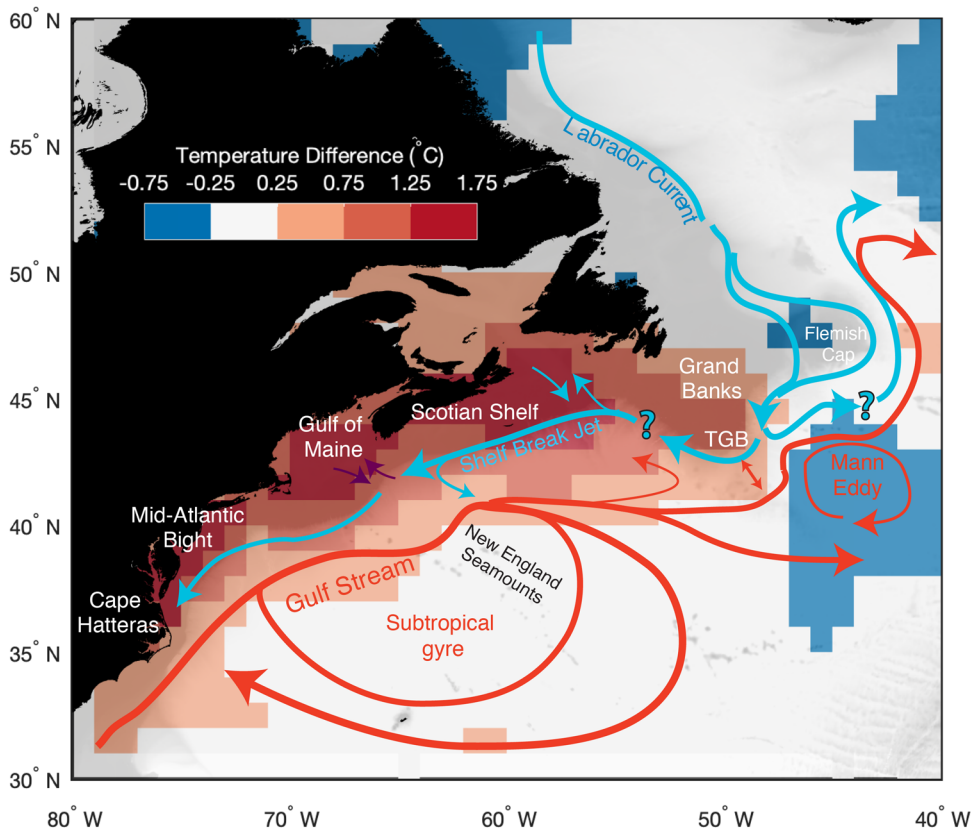

Fig. 1 Schematic of the circulation in the Northwest Atlantic Ocean and the water column average temperature difference between the period 2009–2018 and 2001–2007. The red (blue) shading indicates warming (cooling) of the vertically averaged ocean temperature from the EN4 objective analysis to 2000 m, or the seafloor if it is shallower than 2000 m, in 0.5 °C increments (change in the unshaded region is between −0.25 and 0.25 °C). Background in grayscale shows the bathymetry of the region, with darker shades representing shallower areas. The main circulation features that influence the shelf properties are associated with the Gulf Stream (red) and the Labrador Current (blue) systems, as depicted with arrows. The purple arrows show the waters entering the Gulf of Maine are influenced by both current systems. Coastal and shelf areas of interest are indicated. TGB = Tail of the Grand Banks.

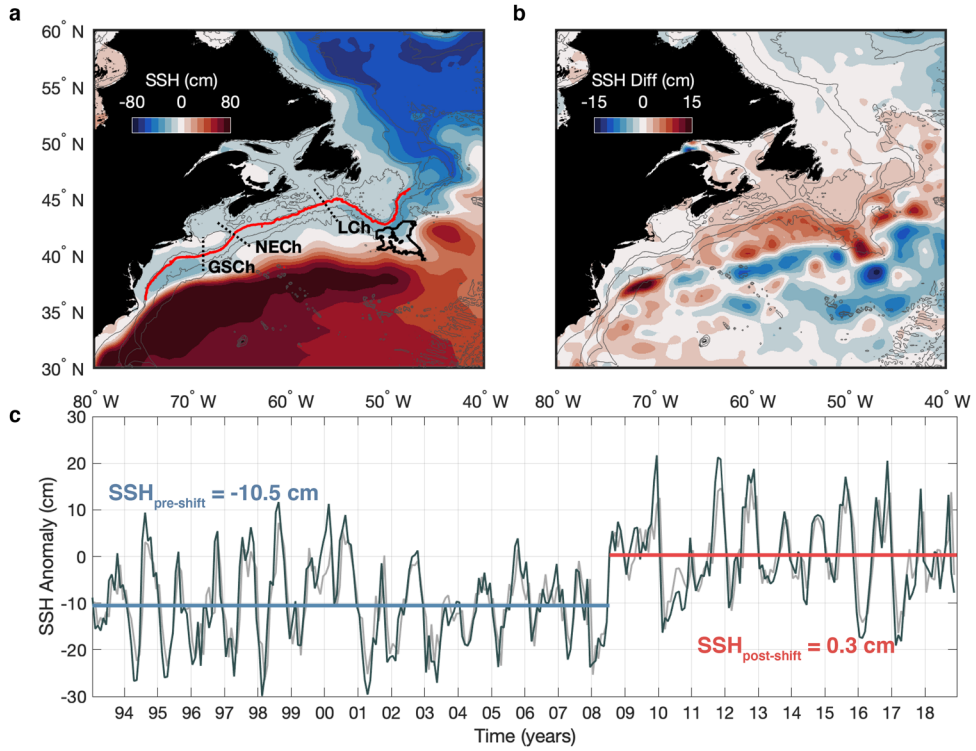

Fig. 2 Sea surface height shift at the Tail of the Grand Banks in 2008. a Mean dynamic topography (MDT) in the Northwest Atlantic between 1993 and 2018. The thick red contour is the 500-m isobath between 76°W and 48°W, along which the along-slope surface velocities displayed in Fig. 3a are calculated. The black dotted lines indicate the main cross-slope channels in the region: Great South Channel (GSCh), Northeast Channel (NECh), and Laurentian Channel (LCh). The 100-m, 1000-m, 3000-m, and 4000-m isobaths are contoured in gray. **b** Sea surface height (SSH) difference between 2009–2018 and 1993–2007. To emphasize spatial patterns, the SSH increase averaged over the entire region that is plotted (equal to 4.5 cm) has been subtracted. **c** Time series of the monthly SSH (dark gray line) and seasonal AutoRegressive Integrated Moving Average (ARIMA) model jointly fit with a change point (light gray line, estimated as described in the "Methods" section) at the Tail of the Grand Banks (i.e., averaged within the thick black contour in panel (**a**). The blue and red horizontal lines indicate the averaged SSH of −10.5 and 0.3 cm before and after the shift, respectively, in July of 2008. Colormaps in panels (**a**) and (**b**) are from the Cmocean package[59].

Results and discussion

Sea level shift at the Tail of the Grand Banks. The strength and position of the Gulf Stream and Labrador Current can be tracked via satellite observations of sea surface height (SSH). The Gulf Stream Extension, with the 25 cm SSH contour marking its axis[21–23], approaches the TGB as a freely meandering jet at 50°W and, on average, aligns with the 4000-m isobath south of the TGB (Fig. 2a). The Gulf Stream can impinge on the slope at the edge of the TGB, thus increasing the SSH inshore of the 4000-m isobath, or meander away from it. Therefore, to evaluate the presence of the Gulf Stream at the TGB, we quantify the SSH variability in the area inshore of the 4000-m isobath (Fig. 2c). In the summer of 2008, a shift toward higher SSH suggests that the Gulf Stream migrated to a position closer to the TGB. This shift has persisted for more than a decade, with an increase in the mean SSH of 10.8 cm for 2009–2018 as compared to 1993–2007, detected beyond the 95% confidence level via change-point analysis (Supplementary Fig. 1; see "Methods"). Accordingly, the Grand Banks has experienced anomalously high sea levels since 2009.

We searched for and quantified the SSH change point specifically at the TGB because the Labrador Current and Gulf Stream are known to interact at this bathymetric feature[24]. The difference in average SSH before and after 2008 shows a dipole pattern with large positive anomalies along and just shoreward of the 4000-m isobath at the TGB, and negative anomalies in deeper waters (Fig. 2b). Although the dipole-like structure is strongest just offshore of the TGB, it extends as far west as the New England Seamounts along the overall (1993–2018) mean axis of the Gulf Stream. This pattern coincides with an increased amplitude in the variability of the Gulf Stream North Wall position east of 50°W after 2005 (Ref. [25]), an increase in the frequency of Gulf Stream deep cyclones after 2008 (Ref. [23]), and is consistent with evidence that the Gulf Stream's path and speed have significantly changed to the east of the New England Seamounts during the altimetry era[26,27]. In contrast, the SSH and the depth-integrated water temperature north of the Grand Banks along the Labrador Current show no difference between the period before and after the shift, despite the observed sea surface warming in this region[3]. In other words, neither water column temperature (Fig. 1) nor SSH (Fig. 2b) indicate that changes at the TGB are driven by changes in the Labrador Current from the Labrador Sea to Flemish Cap.

Temperature anomalies on the Northwest Atlantic Shelf. The presence of the Gulf Stream at the TGB has consequences for the continuity of the Labrador Current west of the Grand Banks. The Labrador Current originates as a western boundary current at the edge of the Labrador shelf and flows southward along the Newfoundland shelf break and through the Flemish Pass before it reaches the TGB. At the TGB, the current bifurcates and some of its volume is transported northeastward inshore of the North Atlantic Current[28] at an estimated rate as large as 2.6 Sv[29,30]. The remainder continues to follow the shelf break west of the Grand Banks as the Shelf Break Jet and can still be seen at the Northeast

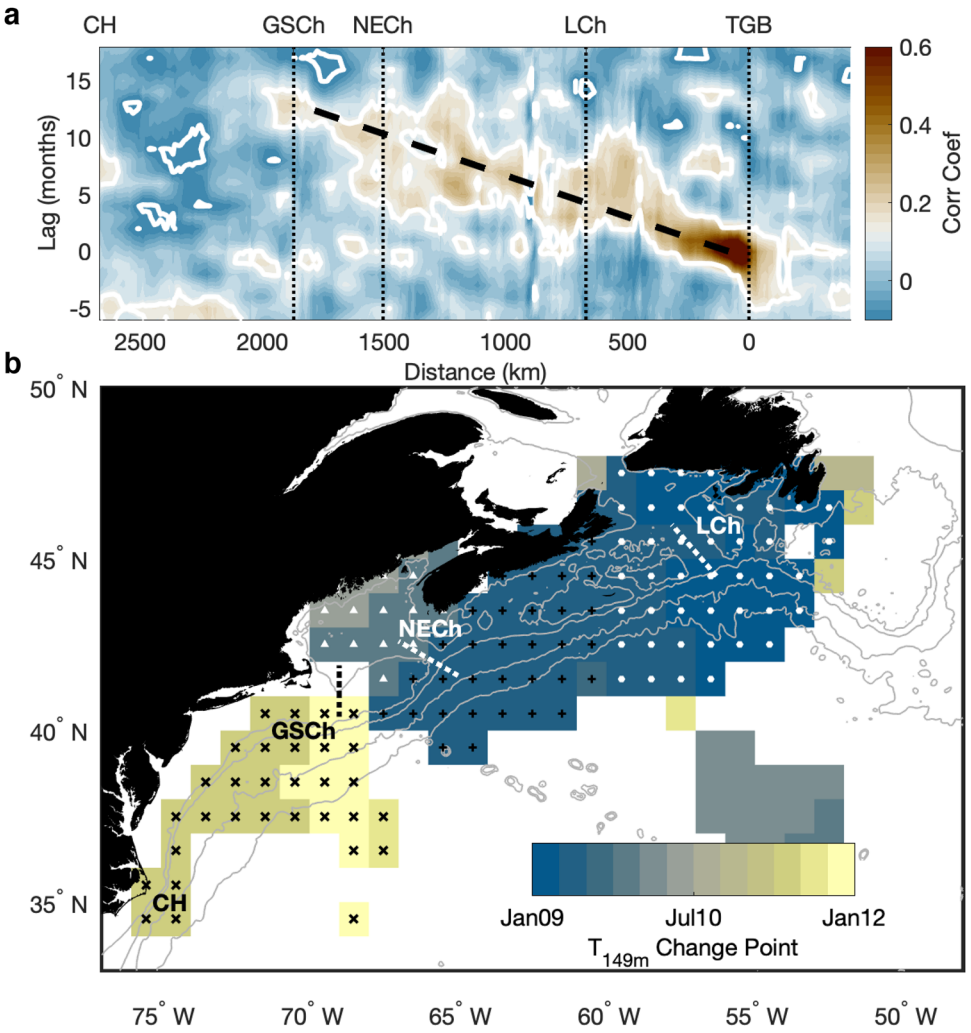

Fig. 3 Along-slope velocity and temperature change west of the Tail of the Grand Banks. a The correlation coefficient between the deseasonalized along-slope surface velocity at the Tail of the Grand Banks of Newfoundland (along the 500-m isobath, at 42°51′N, 50°40′W) and the deseasonalized along-slope surface velocity downstream toward the Northwest Atlantic Shelf (i.e., along the red line in Fig. 2a) as a function of time lags and distance from the Tail of the Grand Banks. White contours represent the 95% significance level. The dashed black line represents a propagation speed of 130 km month^{-1} (5 cm s^{-1}). **b** Map of change-point timing of the 149-m temperature in the Northwest Atlantic. The shades only show grid points whose single change point during 1993–2018 occurred between January/2009 and December/2011. The temperature changes, in °C, associated with these shifts are displayed in Supplementary Fig. 3. Colors are displayed in 3-month intervals. The various hatch marks indicate the grid points used to calculate the regional lagged correlations shown in Table 1: Laurentian Channel (white circles), Scotian Shelf (black plus signs), Gulf of Maine (white triangles) and Mid-Atlantic Bight (black x-marks). The 100-m, 1000-m, 3000-m, and 4000-m isobaths are contoured in gray. The main cross-shelf features are identified. TGB = Tail of the Grand Banks; LCh = Laurentian Channel; NECh = Northeast Channel; GSCh = Great South Channel; CH = Cape Hatteras. Colormaps are from the Crameri package[60].

Channel of the Gulf of Maine[17,31], as schematized in Fig. 1. At the ocean's surface, the current speed along the shelf break can be estimated from the gradient of the SSH field across the shelf break (Supplementary Fig. 2), assuming geostrophic balance. Here, we use satellite altimetry to estimate the variability of the Shelf Break Jet along the 500-m isobath between Flemish Pass and Cape Hatteras. The 500-m isobath was chosen because it is the shallowest isobath (in multiples of 100 m) that continuously follows the shelf break between Flemish Pass and Cape Hatteras (i.e., this isobath does not enter the Gulf of St. Lawrence or the Gulf of Maine). Anomalies in the Shelf Break Jet velocity are significantly correlated with the velocity anomalies at the TGB over a distance of more than 2000 km and at lag times consistent with the advective speed of the Shelf Break Jet (Fig. 3a). The signal continuity persists to the southwest beyond the Laurentian Channel and the Northeast Channel of the Gulf of Maine, only breaking down at the Great South Channel. In contrast, Labrador Current anomalies north of the TGB are uncorrelated with velocity anomalies at the TGB and farther to the southwest, further suggesting that the circulation variability along the Northwest Atlantic Shelf break originates at the TGB and not in the Labrador Sea.

The significant lagged correlations in Fig. 3a provide a means of quantifying the downstream propagation speed of anomalies originating at the TGB. A velocity anomaly along the shelf break takes, on average, nearly 1 year to reach the Great South Channel, which means that it propagates at about 130 km month^{-1} (or 5 cm s^{-1}). Given that (1) higher SSH at the TGB is associated with lower velocities along the shelf break west of the Grand Banks of Newfoundland, and that (2) the SSH at the TGB has

Table 1 Sea surface height and temperature lagged correlations.

		Mid-Atlantic Bight	Gulf of Maine	Scotian Shelf	Laurentian Channel
Raw time series	Correlation coefficient	**0.50**	**0.50**	**0.50**	**0.45**
	Time lag (months)	26	14	13	11
Prewhitened time series	Correlation coefficient	*0.19*	**0.20**	**0.21**	**0.20**
	Time lag (months)	24	14	14	10

Maximum correlation coefficients and time lags between the raw and prewhitened monthly sea surface height at the Tail of the Grand Banks and the monthly 149-m temperature averaged over each of the regions indicated in Fig. 3b, for 1993–2018. Correlation coefficients in bold and italic fonts are significant at the 99.9% and 99% confidence levels, respectively.

been at a higher state since July of 2008, we expect a decrease in the supply of relatively cold/fresh Labrador waters to the shelf and slope following this shift.

Indeed, temperatures on the Northwest Atlantic Shelf apparently responded to the abrupt sea level increase at the TGB in the summer of 2008, as indicated by strong column-integrated warming (color contours in Fig. 1; see also Supplementary Fig. 3). The timing of the warming on the shelf depends on its proximity to the TGB, as expected from the propagation timescale of the velocity anomalies along the shelf break. Change-point analysis reveals that subsurface warming occurs at increasing lag with distance from the TGB (Fig. 3b), a result that is robust for all depths between 100 and 200 m (Supplementary Fig. 4). In the spring of 2009, the Laurentian Channel experienced the onset of high temperature anomalies that have persisted through the end of our analysis (December 2018). By the summer of 2009, the warming reached the slope and shelf offshore of the Gulf of Maine. In subsequent months, the warm subsurface waters were swept into the Gulf of Maine through the continuous inflow on the northwest side of the Northeast Channel[32]. The magnitude of the subsurface warming reached 2.5 °C in the Laurentian Channel and exceeded 1 °C in most of the Gulf of Maine (Supplementary Fig. 3). By the end of 2010, warmer subsurface waters enveloped the entire Northwest Atlantic Shelf between the Great South Channel and the Laurentian Channel.

In agreement with the observed warming on the shelf, a recent analysis inferred that the proportion of Labrador Slope Water entering the Gulf of Maine has been below average since 2010 (except for 2014) and reached a record low in 2017 and 2019, when essentially all of the Gulf of Maine slope water in the Northeast Channel was Warm Slope Water[33]. Simultaneously, the Gulf of Maine and George's Banks experienced rising bottom temperatures[6]. The increased proportion of Warm Slope Water in the Gulf of Maine at the expense of Labrador Slope Water may reinforce atmospherically driven marine heat waves, like the unprecedented surface warming in the first half of 2012[4,5].

South of the Great South Channel, the temperature shift is unlikely the direct result of the anomaly propagation from the TGB. In the Mid-Atlantic Bight, the significant warming shift shown in Fig. 3b occurred after a 1-year lag following the warming on the Scotian Shelf, which is 8–10 months longer than if the anomaly propagated to this region at a speed of approximately 5 cm s^{-1} (the speed of the black dashed line in Fig. 3a). The breakdown of the coherent propagation downstream of the Great South Channel is consistent with a water mass analysis[31] that showed a strong discontinuity in mean temperature and salinity, with a much warmer and saltier shelf break front along the Mid-Atlantic Bight, likely influenced by its close proximity to the Gulf Stream. This discontinuity suggests that other ocean processes likely influence subsurface temperature fluctuations here. For example, the warming after 2011 in this region may be linked to the increased frequency of warm core rings shed by the Gulf Stream and/or northward shifts in the Gulf Stream orientation downstream of the separation point near Cape Hatteras[34–36], in addition to anomalies in surface heat flux[5].

The association of the high SSH anomalies at the TGB and the rapid warming of the Northwest Atlantic Shelf after 2008 was not a one-off event. Between 1993 and 2018, the time series of SSH anomalies at the TGB was significantly correlated at the 99.9% confidence level with the subsurface temperature on the shelf (Table 1; temperatures are averaged over the four regions indicated in Fig. 3c), leading at timescales consistent with the propagation speed of the Labrador Current to the Great South Channel. The progressive lead time of the correlations from the Laurentian Channel (11 months) to the Scotian Shelf (13 months), and Gulf of Maine (14 months) reinforces the westward propagation of temperature anomalies between the Grand Banks and the Northwest Atlantic Shelf. Moreover, the correlations remain significant beyond the 99% level, though smaller in magnitude, at similar lead times after prewhitening (signal shown in Supplementary Fig. 1b). The prewhitening procedure removes all autocorrelation as well as the change point. Thus, the robustness of the correlations to this procedure indicates that the association of SSH anomalies at the TGB and the shelf temperature anomalies is ubiquitous throughout the satellite altimetry era and is not tied only to the 2008 change point or to similarities in seasonal patterns. The association at a lag of about 2 years between the signal at the TGB and the temperature of the Mid-Atlantic Bight is also robust to prewhitening.

The advent of satellite altimetry and the surge in the number of subsurface temperature/salinity measurements on the Northwest Atlantic Shelf in recent decades[37,38] shows that the 2008 circulation shift at the TGB likely set off propagating velocity anomalies along the shelf break and shelf warming. Thus, monitoring sea level anomalies at the TGB may help predict impending shelf temperature anomalies with up to a year of lead time. Additionally, the long history of hydrographic surveys in the Northwest Atlantic allows us to place this recent warming event in the context of the long-term variability of subsurface water masses before the satellite altimetry era.

Centennial-scale shelf warming. The TGB has been monitored for iceberg activity since the International Ice Patrol was formed in response to the sinking of the RMS Titanic in 1912 (Ref. [39]). As such, it has one of the longest oceanographic records of temperature and salinity anywhere. Here, we look at the historical hydrographic records stretching back nearly a century, to put the 2008 shift in a broader context (Fig. 4). For this purpose, a temperature–salinity (T–S) diagram is useful, as these water properties are conserved beneath the ocean's surface and change only through mixing. Thus, a T–S diagram reveals the provenance of different water masses (Fig. 4a; see "Methods" for how the 5153 hydrographic and float profiles were analyzed to reduce the influence of temporal variability in sampling on this diagram). For instance, the cold, fresh Labrador Current north of the TGB

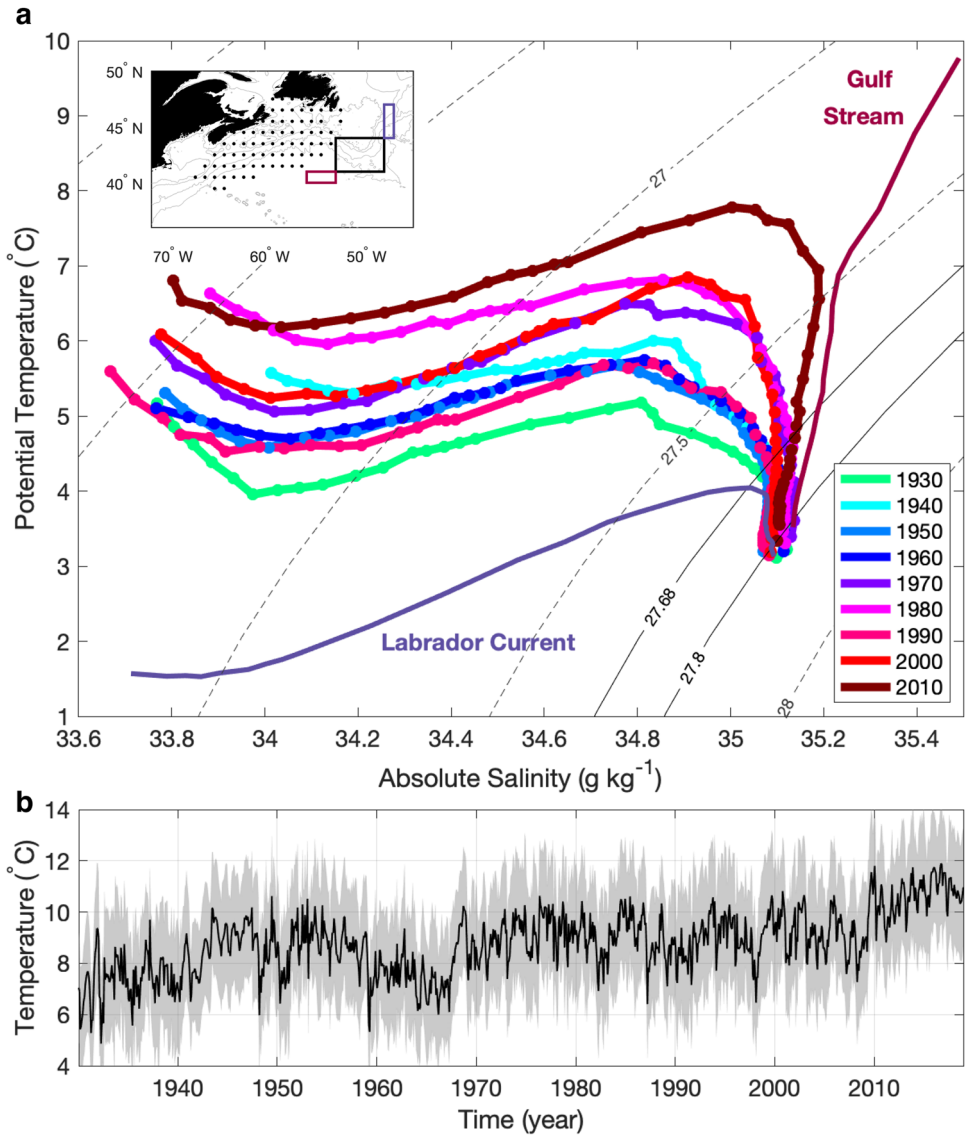

Fig. 4 Temperature–Salinity diagram at the Tail of the Grand Banks and time series of the 149-m temperature on the Scotian Shelf and Laurentian Channel. a Mean decadal profiles of temperature and salinity at the Tail of the Grand Banks between the 1930s and the 2010s are shown as a T–S diagram. The profiles are color-coded by decade of sampling. The blue and red solid lines indicate mean T–S profiles of the Labrador Current and the Gulf Stream, averaged over the blue and red boxes shown in the inset map, respectively. Thin, black lines are the potential density anomalies referenced to the sea surface, with the 27.68 isopycnal (i.e., potential density of 1027.68 kg m^{-3}) and 27.80 isopycnal indicating the upper and lower boundaries of the Labrador Sea Water. A robust locally estimated scatterplot smoothing is applied to the nine decadal profiles at the Tail of the Grand Banks to reduce the effect of outliers at poorly sampled depths. The strategy used to create this diagram while minimizing the influence of variability in the location where the profiles were collected is described in the "Methods" section. **b** Monthly time series of the 149-m temperature averaged over the Scotian Shelf and Laurentian Channel (grid points marked with black dots in the inset map). Gray shades indicate the error estimate averaged over the respective grid points, calculated as shown in the "Methods" section.

contrasts strongly with the warm, salty Gulf Stream. All of the decadally averaged T–S profiles at the TGB are within the envelope bounded by the Labrador Current and the Gulf Stream mean profiles in the layers shallower than the Labrador Sea Water.

The T–S diagram indicates that the last 10 years are uniquely warm and salty compared to any time in the past 80 years. However, a shift to warmer and saltier water masses in the 1970s was of similar scale to this recent shift, relative to decades that preceded it. This warming and salinification in the 1970s may have been caused by a shift of the Gulf Stream toward the TGB, analogous with the more recent change evidenced from the 2008 rise in SSH (Fig. 2). While the shallower water masses of the thermocline have become warmer and saltier, consistent with more frequent incursions of the Gulf Stream onto the TGB, the temperature and salinity of the deep-water masses, like the Labrador Sea Water, have not changed dramatically or monotonically.

The coldest and freshest decades at the TGB occurred between the 1930s and 1960s, only returning to these conditions briefly in the 1990s. The 1990s were extraordinary in this region for a number of reasons. The wintertime deep convection in the Labrador Sea was the strongest since at least the end of the 1930s[40,41], which resulted in the coldest, freshest and thickest

Labrador Sea Water layer on record. Anomalously strong wintertime zonal winds in the subpolar North Atlantic in the early 1990s, expressed as a strong, positive North Atlantic Oscillation (NAO) index[42], helped drive this convection. This cold period lasted only for the first half of the decade; by the late 1990s, the temperature at the TGB returned to the warmer conditions of the post-1970s (Supplementary Fig. 5).

On the Scotian Shelf and the Laurentian Channel, the subsurface temperatures have followed a similar signal as the TGB over the past 9 decades (Fig. 4b, temperature averaged over the grid points marked with black dots in the inset of Fig. 4a). Between 1930 and 1970, the annual mean subsurface shelf temperatures fluctuated widely, with the 1930s and the 1960s being the coldest decades on record (average ± standard deviation of 7.3 ± 0.9 °C and 7.7 ± 0.9 °C, respectively), separated by an intervening warmer period (1940s–1950s, averaging 8.5 ± 0.9 °C). At the end of the 1960s, rapid warming caused the mean annual shelf temperatures to exceed 9.5 °C for the first time in 1968, a state that persisted with little variation for nearly 40 years (1970s–2000s, averaging 9.1 ± 0.8 °C). In 2009, a second warming event raised the shelf temperature by another 1.6 °C (2010–2018, averaging 10.7 ± 0.7 °C). The subsurface shelf waters since 2012 were warmer than ever previously recorded.

The post-2008 dynamical connection established in Figs. 2 and 3, which links SSH anomalies at the TGB to propagating downstream velocity anomalies and shelf warming, is evident in the TGB T–S time series and Scotian Shelf temperatures (Fig. 4). We speculate that similar dynamics were operating earlier in the 20th century, when the appearance of warm and salty waters at the TGB in the 1970s coincides with warming all along the Northwest Atlantic Shelf. It is unclear if this earlier shift was part of a multidecadal oscillation, yet it is notable that only during the high NAO of the early 1990s did the Scotian Shelf or TGB experience a period nearly as cool or fresh as the 1930s–1960s, and the warming after 2008 started from this warmer baseline.

Conclusions

In this study, satellite-based and in situ observations show the influence of the Gulf Stream on the supply of cold, fresh waters from the Labrador Sea to the Northwest Atlantic Shelf. A heightened presence of the Gulf Stream at the TGB after 2008, revealed by a significant warming (Fig. 1), salinification (Fig. 4), and an increase in SSH (Fig. 2), was associated with subsurface warming along the continental shelf and slope between Nova Scotia and Cape Hatteras after 2009 (Fig. 3b, Supplementary Figs. 3 and 6, and Table 1). The more frequent impingements of the Gulf Stream at the Tail of the Grand Banks limited the advective connection of the Labrador Current along the edge of the Northwest Atlantic Shelf, thereby reducing the supply of cold, fresh and oxygen-rich waters to the shelf. This perturbation caused anomalies to propagate along the slope and arrive at the Gulf of Maine nearly 1 year after the appearance of anomalous properties at the TGB.

Additionally, our analysis of nearly a century of hydrographic data suggests that a similar shift toward more subtropical water at the TGB was linked to shelf warming at the end of the 1960s, from which the system had never fully recovered. This long-term record lends support to the hypothesis, based largely on climate modeling, of a 20th century slowdown in the AMOC, which is correlated with the warming of the Northwest Atlantic Shelf[7] and associated with a northward shift of the Gulf Stream and retreat of the Labrador Current[8]. Idealized models predict a northward migration of the Gulf Stream accompanying AMOC slowdowns[43], in line with our observation of the Gulf Stream increasingly impinging on the TGB during shelf warming. In fact, the TGB has been called the "pacemaker" region for the AMOC, and simple dynamical arguments call for AMOC slowdowns to be accompanied by SSH increases at this boundary region[44], as observed following 2008 and inferred in the late 1960s from our water mass analysis (Fig. 4).

The recent subsurface warming of the Northwest Atlantic Shelf, associated with a dynamic change at the TGB, coincides with unprecedented surface warming[1], salinification[45], and severe marine heat waves[46,47] that have likely contributed to long-noted trends in fisheries[1,14,48–50]. Our findings not only help to interpret the rapid temperature fluctuations on the shelf, they also present an opportunity to enhance predictability of future warming. Accurately simulating Gulf Stream–Labrador Current interactions at the TGB appears to be crucial to reproducing the last century of shelf warming, and, therefore, will likely help govern the future properties in this region. Furthermore, monitoring the impingement of the Gulf Stream at the TGB offers up to 1 year of lead time for warming events on the Northwest Atlantic Shelf, and these predictive capabilities may be valuable for forecasting ecosystem changes of consequence for fisheries management.

Methods

Satellite altimetry. Altimetric data is derived from satellite observations with Topex/Poseidon (1992–2002), Jason I (2001–2012), and Jason II (2008–present) and made freely available through the Copernicus Marine Environment Monitoring Service (CMEMS, https://resources.marine.copernicus.eu/). The monthly 0.25° × 0.25° gridded absolute dynamic topography between January 1993 and December 2018 is used to calculate the mean SSH in the region bounded by 30°N, 60°N and 80°W, 40°W, as well as the SSH differences following the 2008 shift. The SSH time series at the TGB is calculated by averaging the absolute dynamic topography over the region highlighted with a thick black contour in Fig. 2a.

The monthly 0.25° × 0.25° gridded surface geostrophic velocity, calculated from the gradient of the SSH between January 1993 and December 2018 provides a measure of the surface Shelf Break Jet speed. The surface geostrophic velocity is interpolated onto the 500-m isobath between Flemish Pass and Cape Hatteras, as indicated by the red contour in Fig. 2a, using a piecewise linear approximation. At each grid point along the 500-m isobath, the surface geostrophic velocity is decomposed into along-slope and across-slope components, with positive values pointing toward Cape Hatteras (along-slope) and inshore (across-slope). The direction of the along-slope component is estimated based on the angle between one grid point on the contoured isobath and the nearest point downstream (i.e., toward Cape Hatteras). Its magnitude is then calculated by projecting the surface geostrophic velocity vector onto the along-slope direction. Similarly, the magnitude of the across-slope component is calculated by projecting the velocity vector onto the across-slope direction. Supplementary Fig. 2 illustrates the direction and magnitude of the all-time mean surface geostrophic velocity as projected onto these components. The along-slope velocity is considered the surface Shelf Break Jet speed used to calculate the lagged correlations shown in Fig. 3a.

EN4 profiles. Historical hydrographic and float profile data compiled and made freely available by the Met Office Hadley Centre (https://www.metoffice.gov.uk/hadobs/en4/) are used to probe the multidecadal variability of water mass composition at the TGB from the 1930s to the present[51]. A total of 5153 profiles taken in April, May, or June within the box 41°N–44°N, 48°W–53°W were analyzed (Supplementary Fig. 6 shows the location of the profiles used for each decade). Pre-ARGO profiles have been historically biased toward these months, and this subset represents 51% of all profiles taken in this region. We avoid aliasing seasonal variability in our multidecadal time series by limiting our analysis to a single well-sampled season[20]. Poor data was removed based on EN4's quality-control flag system, and only data points with accepted pairs of potential temperature and practical salinity were used. Each profile was linearly interpolated to a maximum of 55 vertical levels, with 5-m resolution in the top 100 m, 25-m resolution above 250 m, 50-m resolution above 1550 m, and 250-m resolution above 2050 m. The maximum depth of the averaged profiles is 2050 m, as less than 2% of the profiles in the region reach greater depths.

To avoid the aliasing of variability in the location where the profiles were collected in the TGB box, we subtract an appropriate gridded all-time mean T–S profile from each individual observation, as follows. The profiles were bin-averaged into 30 boxes of 0.5° latitude × 1° longitude with a terrain-following penalty, λ, which sets the "effective distance" between the location of each profile and the center of each box, thereby clustering profiles collected at similar isobaths. The

squared effective distance was calculated as

$$D_{\mathrm{eff}}^2 = \left[\left(x_\mathrm{b} - x_\mathrm{p}\right)^2 + \left(y_\mathrm{b} - y_\mathrm{p}\right)^2\right] + \left[3\lambda\left(\frac{H_\mathrm{b} - H_\mathrm{p}}{H_\mathrm{b} + H_\mathrm{p}}\right)\right]^2 \quad (1)$$

where λ is set to 1 km, and $(x_\mathrm{b}, y_\mathrm{b})$ and $(x_\mathrm{p}, y_\mathrm{p})$ are the location of the center of the box and the profile, respectively. H_b and H_p are the depths at those locations, estimated from ETOPO-1[52]. This penalty lengthens bins in their along-isobath direction and shortens them in the across-isobath direction, which is a more dynamic way to subdivide this region, given that the currents are steered by steep topography[53,54].

Once each profile was assigned to one of these 30 terrain-following bins, we averaged the profiles taken in the same bin and month, to avoid giving disproportionate weight to correlated profiles collected very close to one another in space and time. Then, we calculated all-time, bin mean profiles:

$$\bar{T}_{x,y} = \frac{1}{N_{x,y}}\sum_{i=1}^{N_{x,y}} T_{i(x,y)},\ \bar{S}_{x,y} = \frac{1}{N_{x,y}}\sum_{i=1}^{N_{x,y}} S_{i(x,y)} \quad (2)$$

where $T_{i(x,y)}$ and $S_{i(x,y)}$ are the temperature and salinity profiles (either individual profiles or the pre-averaged profiles collected in a given bin and month), numbering N quasi-independent profiles in each x, y bin. Anomaly profiles were then calculated by subtracting the all-time, bin mean $(\bar{T}_{x,y}, \bar{S}_{x,y})$ from each profile in the corresponding bin $(T_{i(x,y)}, S_{i(x,y)})$:

$$T'_{i(x,y)} = T_{i(x,y)} - \bar{T}_{x,y},\ S'_{i(x,y)} = S_{i(x,y)} - \bar{S}_{x,y} \quad (3)$$

A decadal-mean anomaly profile $(\bar{T}'_{\mathrm{decade}}, \bar{S}'_{\mathrm{decade}})$ was calculated by averaging the resulting anomalies from Eq. (3) over the entire TGB region for each of the 9 decades. Finally, the all-time, spatially averaged mean profile was added back to the decadal anomalies to calculate the mean decadal profiles:

$$\bar{T}_{\mathrm{decade}} = \bar{T}'_{\mathrm{decade}} + \frac{1}{N_{x,y}}\sum_{i=1}^{N_{x,y}} T_i, \bar{S}_{\mathrm{decade}} = \bar{S}'_{\mathrm{decade}} + \frac{1}{N_{x,y}}\sum_{i=1}^{N_{x,y}} S_i \quad (4)$$

We apply the same method to calculate the all-time mean profiles in the Labrador Current (44°N–47°N, 48°W–47°W) and Gulf Stream (40°N–41°N, 56°W–53°W) domains at a 10-m vertical resolution, as shown in solid lines in Fig. 4a.

EN4 objective analysis. The monthly 1° × 1° objective analysis gridded product with 42 vertical levels[51,55], made freely available by the Met Office Hadley Centre (https://www.metoffice.gov.uk/hadobs/en4/), is derived from the hydrographic and float dataset described above. The temperature field at 149 m in the region bounded by 33°N, 50°N and 77°W, 48°W is used in the change-point analysis described below. Here, the period analyzed is January 1993 to December 2018, coincident with the altimetric data. Twelve additional layers between 56 and 235 m were also analyzed to determine the vertical extent of the changes observed at 149 m.

Decadal changes in the 149-m layer are analyzed in the time series extending back to 1930 (Fig. 4b). The authors of the EN4 objective analysis highlight that this dataset should be used with caution in the analysis of long-term trends, because, during periods with few observations, the analyses relax to climatology[51]. Supplementary Fig. 7 shows that the Northwest Atlantic has been historically well-observed, as the number of profiles is plotted in a 1° × 1° grid. Over 1.3 million profiles were used to build the objective analyses here, most of which were taken on the shelf and slope. The error estimate in Fig. 4b is calculated at each time-step t as

$$E = \sqrt{\frac{1}{N}\sum_{x=1}^{N}\sigma_x^2 + \frac{1}{N}\sum_{x=1}^{N}U_{x,t}^2} \quad (5)$$

where σ_x and $U_{x,t}$ are the standard deviation and objective analysis uncertainty estimate of the 149-m temperature at each of the N grid points, respectively.

Change-point analysis. The 2008 shift in the 1993–2018 SSH time series at the TGB is characterized using a seasonal AutoRegressive Integrated Moving Average (ARIMA) model, which explains the SSH based on its own past values (i.e., its own lags and lagged observation errors). We jointly fit a seasonal ARIMA with each possible monthly change point, iterating over all months between January 1997 and December 2014. The timing of the SSH shift is selected as the month at which inserting a change point maximizes the model log-likelihood, and its inclusion is verified by comparing the Akaike information criterion (AIC) to a model without a change point. All change-point analyses are conducted in R[56] using the "forecast" package[57]. The orders of the resulting seasonal ARIMA, chosen via stepwise selection using the AIC, were $(2,0,0) \times (2,0,0)_{12}$. These orders indicate that the SSH time series is mean stationary, aside from the jointly fit level shift, with significant autocorrelation at 1-, 2-, 12-, and 24-month lags, as seen in Supplementary Fig. 1b. These lags are consistent with strong month-to-month and seasonal signals. The temporal autocorrelation structure explains 45.8% of the variability in the time series, and the change point explains an additional 24.1%.

Similar to the analysis of the SSH at the TGB, temperature change points between January 1997 and December 2014 on the Northwest Atlantic Shelf are identified jointly with a seasonal ARIMA model, for each 1° × 1° grid cell between 30–60°N and 40–80°W. The maximum orders we allowed for these seasonal ARIMA models are $(1,0,1) \times (1,1,1)_{12}$, chosen under the assumption that the temperature observations 1 month and 1 year prior to a measurement contain all available information for estimation. We also assume that the temperature time series are mean stationary after accounting for any change points, and therefore do not model a non-seasonal integrated process. However, variation in the magnitude of the seasonal cycle is permitted. Candidate temperature change points are selected as those that maximize the 3-month running mean of the model log-likelihood, in order to avoid choosing isolated, sharp peaks in the likelihood function, and are retained if they both reduce the AIC over a model without a change point and occur between the SSH shift at the TGB (July, 2008) and December, 2011. We chose this window to identify only temperature change points that followed the SSH shift at the TGB, considering the time lags associated with the propagation speed of the Labrador Current described in Fig. 3a.

To study the relationship between temperature change points detected in different regions of the Northwest Atlantic Shelf and the SSH shift at the TGB, mean temperature time series are calculated for areas of grid cells exhibiting similar change-point timing (hatch marks in Fig. 3b). To prewhiten the SSH and regional temperature time series, we filter using the SSH seasonal ARIMA model fit, including the change point, using the R package "TSA"[58]. For both the raw and prewhitened time series, the strength and time lag of the correlations between the SSH at the TGB and the mean temperature of each identified region are evaluated (Table 1).

Data availability

Altimetric data is derived from satellite observations with Topex/Poseidon (1992–2002), Jason I (2001–2012), and Jason II (2008–present) and made freely available through the Copernicus Marine Environment Monitoring Service (CMEMS, data can be accessed here upon registration). The historical hydrographic and float profile data, as well as the derived 1° × 1° monthly objective analyses gridded product, are compiled and made freely available by the Met Office Hadley Centre (data can be accessed here).

Code availability

The MATLAB code written to load and analyze the data and to generate the figures is available at https://github.com/afonsogneto/Matlab. The R codes used in the change-point analysis are referenced in the "Methods" section and listed in the bibliography.

Received: 22 September 2020; Accepted: 16 March 2021;
Published online: 20 April 2021

References

1. Pershing, A. J. et al. Slow adaptation in the face of rapid warming leads to collapse of the Gulf of Maine cod fishery. *Science* **350**, 809–812 (2015).
2. National Marine Fisheries Service. *Fisheries Economics of the United States 2016* (NOAA, 2018).
3. Chen, Z. et al. Long-term SST variability on the Northwest Atlantic continental shelf and slope.*Geophys. Res. Lett.* **47**, e2019GL085455 (2020).
4. Chen, K., Gawarkiewicz, G. G., Lentz, S. J. & Bane, J. M. Diagnosing the warming of the Northeastern U.S. Coastal Ocean in 2012: a linkage between the atmospheric jet stream variability and ocean response. *J. Geophys. Res. Oceans* **119**, 218–227 (2014).
5. Chen, K., Gawarkiewicz, G., Kwon, Y. & Zhang, W. G. The role of atmospheric forcing versus ocean advection during the extreme warming of the Northeast U.S. continental shelf in 2012. *J. Geophys. Res. Oceans* **120**, 4324–4339 (2015).
6. Friedland, K. D. et al. Trends and change points in surface and bottom thermal environments of the US Northeast Continental Shelf Ecosystem. *Fish. Oceanogr.* **29**, 396–414 (2020).
7. Caesar, L., Rahmstorf, S., Robinson, A., Feulner, G. & Saba, V. Observed fingerprint of a weakening Atlantic Ocean overturning circulation. *Nature* **556**, 191–196 (2018).
8. Saba, V. S. et al. Enhanced warming of the Northwest Atlantic Ocean under climate change. *J. Geophys. Res. Oceans* **121**, 118–132 (2015).
9. Gaichas, S. K., Link, J. S. & Hare, J. A. A risk-based approach to evaluating northeast US fish community vulnerability to climate change. *ICES J. Mar. Sci.* **71**, 2323–2342 (2014).
10. Hare, J. A. et al. A vulnerability assessment of fish and invertebrates to climate change on the Northeast U.S. Continental Shelf. *PLoS ONE* **11**, e0146756 (2016).
11. Lauzier, L. M. Long-term temperature variations in the Scotian Shelf area. *ICNAF Spec. Publ.* **6**, 807–816 (1965).

12. Nye, J. A., Joyce, T. M., Kwon, Y.-O. & Link, J. S. Silver hake tracks changes in Northwest Atlantic circulation. *Nat. Commun.* **2**, 412 (2011).
13. Pershing, A. J. et al. Oceanographic responses to climate in the Northwest Atlantic. *Oceanography* **14**, 76–82 (2001).
14. Davis, X. J., Joyce, T. M. & Kwon, Y.-O. Prediction of silver hake distribution on the Northeast U.S. shelf based on the Gulf Stream path index. *Cont. Shelf Res.* **138**, 51–64 (2017).
15. Le Bris, A. et al. Climate vulnerability and resilience in the most valuable North American fishery. *Proc. Natl. Acad. Sci. USA.* **115**, 1831–1836 (2018).
16. Schartup, A. T. et al. Climate change and overfishing increase neurotoxicant in marine predators. *Nature* **572**, 648–650 (2019).
17. Petrie, B. & Drinkwater, K. Temperature and salinity variability on the Scotian Shelf and in the Gulf of Maine 1945–1990. *J. Geophys. Res.* **98**, 20079 (1993).
18. Gilbert, D., Sundby, B., Gobeil, C., Mucci, A. & Tremblay, G.-H. A seventy-two-year record of diminishing deep-water oxygen in the St. Lawrence estuary: the northwest Atlantic connection. *Limnol. Oceanogr.* **50**, 1654–1666 (2005).
19. Brickman, D., Hebert, D. & Wang, Z. Mechanism for the recent ocean warming events on the Scotian Shelf of eastern Canada. *Cont. Shelf Res.* **156**, 11–22 (2018).
20. Claret, M. et al. Rapid coastal deoxygenation due to ocean circulation shift in the northwest Atlantic. *Nat. Clim. Change* **8**, 868–872 (2018).
21. Lillibridge, J. L. & Mariano, A. J. A statistical analysis of Gulf Stream variability from 18+ years of altimetry data. *Deep Sea Res. II* **85**, 127–146 (2013).
22. Rossby, T., Flagg, C. N., Donohue, K., Sanchez-Franks, A. & Lillibridge, J. On the long-term stability of Gulf Stream transport based on 20 years of direct measurements. *Geophys. Res. Lett.* **41**, 114–120 (2014).
23. Andres, M. On the recent destabilization of the Gulf Stream path downstream of Cape Hatteras: Gulf Stream path destabilization. *Geophys. Res. Lett.* **43**, 9836–9842 (2016).
24. Rossby, T. On gyre interactions. *Deep Sea Res. II* **46**, 139–164 (1999).
25. Seidov, D., Mishonov, A., Reagan, J. & Parsons, R. Resilience of the Gulf Stream path on decadal and longer timescales. *Sci. Rep.* **9**, 11549 (2019).
26. Dong, S., Baringer, M. O. & Goni, G. J. Slow down of the Gulf Stream during 1993–2016. *Sci. Rep.* **9**, 6672 (2019).
27. Andres, M., Donohue, K. A. & Toole, J. M. The Gulf Stream's path and time-averaged velocity structure and transport at 68.5°W and 70.3°W. *Deep Sea Res. I* **156**, 103179 (2020).
28. Rossby, T. The North Atlantic Current and surrounding waters: At the crossroads. *Rev. Geophys.* **34**, 463–481 (1996).
29. Loder, J. W., Petrie, B. & Gawarkiewicz, G. G. The coastal ocean off northeastern North America: a large-scale view. In *The Sea,* Vol.11 (eds. Robinson, A.R. & Brink, K.H.) 105–133 (Wiley, 1998).
30. Fratantoni, P. S. & McCartney, M. S. Freshwater export from the Labrador Current to the North Atlantic Current at the Tail of the Grand Banks of Newfoundland. *Deep Sea Res. I* **57**, 258–283 (2010).
31. Fratantoni, P. S. & Pickart, R. S. The western North Atlantic shelfbreak current system in summer. *J. Phys. Oceanogr.* **37**, 2509–2533 (2007).
32. Ramp, S. R., Schlitz, R. J. & Wright, W. R. The deep flow through the Northeast Channel, Gulf of Maine. *J. Phys. Oceanogr.* **15**, 1790–1808 (1985).
33. Northeast Fisheries Science Center. *2020 State of the Ecosystem: New England* (NOAA, 2020).
34. Gawarkiewicz, G. G., Todd, R. E., Plueddemann, A. J., Andres, M. & Manning, J. P. Direct interaction between the Gulf Stream and the shelfbreak south of New England. *Sci. Rep.* **2**, 553 (2012).
35. Forsyth, J. S. T., Andres, M. & Gawarkiewicz, G. G. Recent accelerated warming of the continental shelf off New Jersey: observations from the CMVOleander expendable bathythermograph line. *J. Geophys. Res. Oceans* **120**, 2370–2384 (2015).
36. Gangopadhyay, A., Gawarkiewicz, G., Silva, E. N. S., Monim, M. & Clark, J. An observed regime shift in the formation of warm core rings from the Gulf Stream. *Sci. Rep.* **9**, 12319 (2019).
37. Toole, J. M., Andres, M., Le Bras, I. A., Joyce, T. M. & McCartney, M. S. Moored observations of the Deep Western Boundary Current in the NWAtlantic: 2004–2014: LINE W 2004–2014. *J. Geophys. Res. Oceans* **122**, 7488–7505 (2017).
38. Smith, L. et al. The Ocean Observatories Initiative. *Oceanography* **31**, 16–35 (2018).
39. IIP. *Report of the International Ice Patrol in the North Atlantic (2019 Season).* 1–123 (Homeland Security, 2019).
40. Yashayaev, I. Hydrographic changes in the Labrador Sea, 1960–2005. *Prog. Oceanogr.* **75**, 857–859 (2007). [Prog. Oceanogr. 73 (2007) 242–276].
41. Yashayaev, I. & Loder, J. W. Recurrent replenishment of Labrador Sea Water and associated decadal-scale variability. *J. Geophys. Res. Oceans* **121**, 8095–8114 (2016).
42. Yashayaev, I. & Loder, J. W. Further intensification of deep convection in the Labrador Sea in 2016. *Geophys. Res. Lett.* **44**, 1429–1438 (2017).
43. Zhang, R. & Vallis, G. K. The role of bottom vortex stretching on the path of the North Atlantic Western Boundary Current and on the Northern Recirculation Gyre. *J. Phys. Oceanogr.* **37**, 2053–2080 (2007).
44. Buckley, M. W. & Marshall, J. Observations, inferences, and mechanisms of the Atlantic Meridional Overturning Circulation: a review. *Rev. Geophys.* **54**, 5–63 (2016).
45. Grodsky, S. A., Reul, N., Chapron, B., Carton, J. A. & Bryan, F. O. Interannual surface salinity on Northwest Atlantic Shelf. *J. Geophys. Res. Oceans* **122**, 3638–3659 (2017).
46. Mills, K. et al. Fisheries management in a changing climate: lessons from the 2012 ocean heat wave in the Northwest Atlantic.*Oceanography* **26**, 191–195 (2013).
47. Pershing, A., Mills, K., Dayton, A., Franklin, B. & Kennedy, B. Evidence for adaptation from the 2016 marine heatwave in the Northwest Atlantic Ocean. *Oceanography* **31**, 151–161 (2018).
48. Nye, J., Link, J., Hare, J. & Overholtz, W. Changing spatial distribution of fish stocks in relation to climate and population size on the Northeast United States continental shelf. *Mar. Ecol. Prog. Ser.* **393**, 111–129 (2009).
49. Dubik, B. A. et al. Governing fisheries in the face of change: Social responses to long-term geographic shifts in a U.S. fishery. *Mar. Policy* **99**, 243–251 (2019).
50. Oremus, K. L. Climate variability reduces employment in New England fisheries. *Proc. Natl. Acad. Sci. USA.* **116**, 26444–26449 (2019).
51. Good, S. A., Martin, M. J. & Rayner, N. A. EN4: quality controlled ocean temperature and salinity profiles and monthly objective analyses with uncertainty estimates. *J. Geophys. Res. Oceans* **118**, 6704–6716 (2013).
52. Eakins, B. E. & Amante, C. *ETOPO1 1 Arc-Minute Global Relief Model: Procedures, Data Sources and Analysis* (NOAA, 2009).
53. Davis, R. E. Preliminary results from directly measuring middepth circulation in the tropical and South Pacific. *J. Geophys. Res. Oceans* **103**, 24619–24639 (1998).
54. Lavender, K. L., Brechner Owens, W. & Davis, R. E. The mid-depth circulation of the subpolar North Atlantic Ocean as measured by subsurface floats. *Deep Sea Res. I* **52**, 767–785 (2005).
55. Gouretski, V. & Reseghetti, F. On depth and temperature biases in bathythermograph data: development of a new correction scheme based on analysis of a global ocean database. *Deep Sea Res. I* **57**, 812–833 (2010).
56. R Core Team. *R: A Language and Environment for Statistical Computing* (R Foundation for Statistical Computing, 2020).
57. Hyndman, R. *et al. forecast: Forecasting functions for time series and linear models. R package version 8.10.* (CRAN, 2019).
58. Chan, K. & Ripley, B. *TSA: Time Series Analysis. R package version 1.2.* (CRAN, 2018).
59. Thyng, K., Greene, C., Hetland, R., Zimmerle, H. & DiMarco, S. True colors of oceanography: guidelines for effective and accurate colormap selection. *Oceanography* **29**, 9–13 (2016).
60. Crameri, F. *Scientific Colour-Maps: Perceptually Uniform and Colour-Blind Friendly* (Zenodo, 2018).

Acknowledgements

J.B.P. gratefully acknowledges funding from NSF OCE-1947829 and the NOAA Climate Variability Program (Project #0008287). All authors appreciate conversations with Kathy Donohue, Tom Rossby, Gavino Puggioni, and Don Rudnickas, which helped to sharpen the ideas and the statistical analyses.

Author contributions

A.G.N. assembled, analyzed, and interpreted the observational data and wrote the first draft of the manuscript. J.A.L. did the change-point analysis, discussed methods, results, and interpretation and helped revise the manuscript. J.B.P. discussed methods, results, and interpretation and helped revise the manuscript.

Competing interests

The authors declare no competing interests.

Additional information

Supplementary information The online version contains supplementary material available at https://doi.org/10.1038/s43247-021-00143-5.

Correspondence and requests for materials should be addressed to A.G.N.

Peer review information Primary handling editors: Joseph Aslin, Clare Davis.

Reprints and permission information is available at http://www.nature.com/reprints

Publisher's note Springer Nature remains neutral with regard to jurisdictional claims in published maps and institutional affiliations.